Electrochemical, morphological and theoretical evaluation of a new poly(3-sulfolene-co-*cis*-2-butene-1,4-dilinoleate) against corrosion of AISI 1020 steel in 0.1 N HCl solution

R.J. Tuama

Department of Chemistry, College of Science, University of Thi-Qar, Thi-Qar 64001, Iraq
E-mail: Rashajasim@utq.edu.iq

Abstract

This research includes the preparation of a new poly(3-sulfolene-co-*cis*-2-butene-1,4-dilinoleate) (PSCOCBDL) by free radical polymerization of the preliminarily prepared *cis*-2-butene-1,4-dilinoleate with 3-sulfolene. This prepared copolymer was diagnosed using Fourier transform infrared spectroscopy and Gel permeation chromatography. The corrosion inhibition effect of poly(3-sulfolene-co-*cis*-2-butene-1,4-dilinoleate) on AISI 1020 steel corrosion in 0.1 N hydrochloric acid solution was studied at a temperature 298 K by means of electrochemical impedance spectroscopy and potentiodynamic polarization techniques. A set of experiments with different concentrations of the inhibitor copolymer (15, 30, 45 and 60 ppm) were conducted. The study revealed that the inhibition efficiency increases with an increase in concentration. Potentiodynamic polarization measurements detected that the PSCOCBDL copolymer was a corrosion inhibitor of anodic type. Atomic force microscopy technique was employed to determine the surface morphology of AISI 1020 steel samples after exposure both in uninhibited and inhibited medium. The morphological study indicated that adsorption of the corrosion inhibitor copolymer PSCOCBDL on AISI 1020 steel surface resulted in building a protective layer. The adsorption of the prepared copolymer on AISI 1020 steel surface obeys the Langmuir isotherm. Various quantum chemical descriptors have been calculated based on the density functional theory, such as E_{HOMO}, E_{LUMO}, ΔE, χ, η, S, and μ, which are related most closely to the anti-corrosive features of the examined copolymer. A molecule with a higher E_{HOMO} can take electrons speedily from an appropriate acceptor molecule with a lower-energy vacuous molecular orbital, while the E_{LUMO} value indicates how well the molecule can hold back electrons.

Received: January 24, 2024. Published: June 6, 2024 doi: 10.17675/2305-6894-2024-13-2-24

Keywords: *copolymer, AISI 1020 steel, electrochemical impedance spectroscopy, potentiodynamic polarization, quantum chemical descriptors.*

1. Introduction

The deterioration of facilities made of steel due to corrosion is a main issue in petrochemical manufactures and in other engineering firms [1, 2], as the annual corrosion results in the closure of numerous factories and cessation of installations, as well as the loss and subsequent damage of numerous industrial products, which ultimately contribute to

environmental contamination [3–5]. In industry, acid solutions are utilized for a variety of purposes, including acid descaling, acid pickling, acid descaling in industry, and acidizing of oil wells. Corrosion assaults ensue due to the acidic solution's inherently corrosive characteristics. As a result, investment initiatives in corrosion management within the metal industry become exorbitantly costly [6, 7]. Therefore, it is fundamental to prepare some powerful corrosion inhibitors. Inhibition by organic compounds comprising heteroatoms N, S and O, especially in the presence of π-electrons in their structures. Organic polymers are among the most efficacious techniques for protection of metals against corrosion when exposed to corrosive acidic environments [8, 9]. This is due to its great liability to form complex compounds with ions of metals and be efficiently adsorbed on surfaces of metals due to the presence of diverse functional groups in the polymer molecules. Polymer molecules or their complexes with metals occupy a significant surface area, that way covering the surface and shielding the metal from corrosive compounds present in the solution [10, 11].

The adsorption mechanism is predicated on polar groups serving as efficient centers for the adsorption process; the adsorption film that is produced serves as a barrier, efficiently segregating the steel substrate from the hostile environments to which it is exposed [12]. Numerous studies have demonstrated that polymers are efficient corrosion inhibitors and coating materials. The synthesis of a collection of polymers was achieved through the reaction of hydroxyquinazoline derivatives and aminoquinazoline derivatives with *N*,*N*-cyclohexyl carbodiimide (DCCI) in the presence of methacrylic acid by Aly *et al*. These polymers were explored as corrosion inhibitors of AISI 1020 steel in HCl media. The protective efficiency was estimated through utilization of potentiodynamic polarization. The findings show that the inhibition efficiency increased with an increase in inhibitor concentration and was reduced with temperature. Inhibition occurred due to adsorption of polymer compounds on the mild steel surface [13]. Various factors that affect corrosion inhibition, including the structure of the molecules and concentration of 1-phenyl-2-thiourea (PTU) and 1,3-diisopropyl-2-thiourea (ITU) in 1.0 M HCl, were examined by Huong *et al*. utilizing PDP curves, EIS and quantum chemical calculations. The inhibitory efficiencies of PTU and ITU at 5×10^{-3} M and 60°C were found to be the highest at 98.96 and 92.65%, respectively. PTU and ITU are adsorbed on the metal surface according to the Langmuir adsorption isotherm. The theoretical results for the inhibitors agree well with experimental data [14]. Rahal *et al*. studied the utilization of thiobarbituric acid (TBA) and thiourea (TU) as corrosion inhibitors of mild steel in 0.5 M HNO_3 by utilizing PDP, EIS and quantum-chemical calculations. Both of these inhibitors displayed perfect inhibition efficiency in the HNO_3 solution. A number of isotherms, namely Langmuir, Flory-Huggins, Temkin and kinetic-thermodynamic models, were used fit data on adsorption of inhibitors on mild steel surface [15].

This present study aims at the synthesis and characterization of a new polymeric compound, poly(3-sulfolene-co-*cis*-2-butene-1,4-dilinoleate) (PSCOCBDL), and its evaluation as a corrosion inhibitor of AISI 1020 steel in 0.1 N HCl. This is due to the high

molecular weight and repeating functional groups of this prepared polymeric compound, which provide higher electron density at the inhibitor's adsorption centers and thus strengthen the interactions between the inhibitor molecules and the metal surface, resulting in protection of the metal from corrosion.

2. Experimental

2.1. Materials

The chemical composition (in *wt.*%) of AISI 1020 steel obtained from company metal samples (United States): 98.5% Fe, 0.2% C, and 0.6% Mn; minor amounts of P, S, Si, Sn, Cu, Ni, Cr and Mo. Sigma-Aldrich in Germany supplied the following chemicals: linoleic acid, 3-sulfolene, *cis*-2-butene-1,4-diol, zinc oxide, benzoyl peroxide, toluene, and hydrochloric acid.

2.2. Synthesis of poly(3-sulfolene-co-cis-2-butene-1,4-dilinoleate)

a. Condensation reaction

Linoleic acid (6.66 ml, 0.021 mol) and *cis*-2-butene-1,4-diol (3.45 ml, 0.042 mol) were reacted *via* condensation reaction in a 100 mL round-bottom flask equipped with a reflux condenser. The reaction was performed at a mole ratio of 1:2, with ZnO serving as the catalyst. A nitrogen atmosphere was used to heat the reaction mixture at 70–80°C for four hours while agitating continuously. Following the completion of this procedure, the product was kept in a separating funnel for 1 h in order to obtain two distinct strata. After eliminating the unreacted substances and water from the lowermost layer, the organic layer at the top was isolated. The product was kept at r.t. for 24 h [16] to give *cis*-2-butene-1,4-dilinoleate (CBDL).

b. Copolymerization

cis-2-Butene-1,4-dilinoleate prepared in advance was copolymerized with 3-sulfolene in toluene at a molar ratio of 1:4 under nitrogen atmosphere with benzoyl peroxide as the initiator (1% w/w). Then, continuous stirring at 70°C for 3 h was used to complete the polymerization. The copolymer thus obtained was dried *in vacuo* for 24 h [17, 18]. Scheme 1 illustrates the PSCOCBDL synthesis.

2.3. Characterization of the synthesized copolymer

The chemical structure of the synthesized copolymer was determined using a Bruker FTIR spectrometer. The Fourier transform infrared spectra (FTIR) were recorded in the 400–4000 cm^{-1} range and analyzed. Gel permeation chromatography (GPC) was employed to ascertain the average molecular weight (Mn) of the copolymer. A refractive index detector was utilized in conjunction with a Breeze™ 2 HPLC System. THF (Merck) was employed as the eluent fed at a rate of 1.0 mL/min.

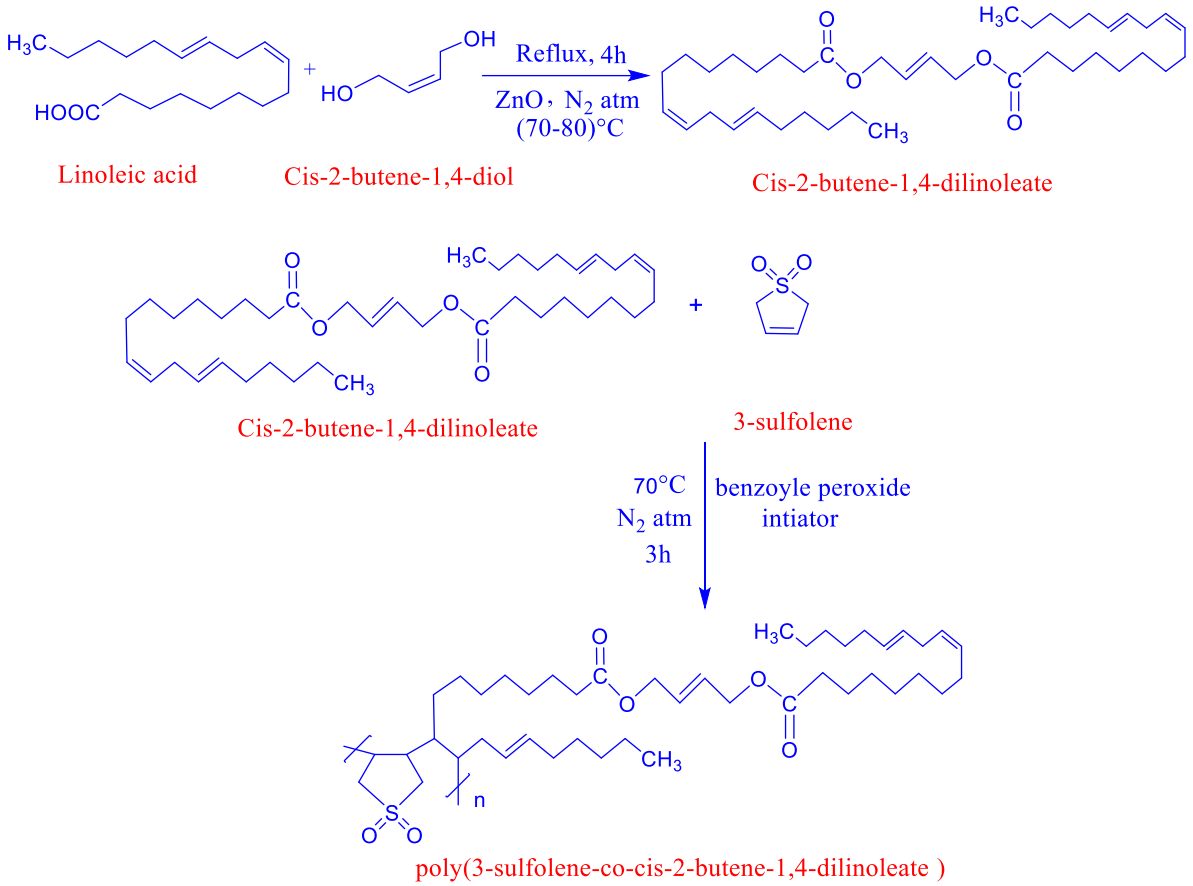

Scheme 1. Schematic illustration of PSCOCBDL preparation.

2.4. Electrochemical measurements

Electrochemical measurements were conducted using an Ivium potentiostat/galvanostat (Vertex One, Ivium Technologies, Netherlands). The experimental setup involved three electrodes arranged in a cell assembly: AISI 1020 steel as the working electrode, a platinum counter electrode, and a saturated calomel (Hg/Hg_2Cl_2 sat. KCl) reference electrode. Samples of AISI 1020 steel were submerged at 298 K in the acid solution comprising 0.1 N HCl and various concentrations of the corrosion inhibitor PSCOCBDL (15, 30, 45, and 60 ppm). Subsequently, electrochemical impedance (EIS) measurements were conducted, yielding impedance spectra with amplitudes of 10 mV and frequencies ranging from 100 kHz to 0.1 Hz. Experiments utilizing potentiodynamic polarization (PDP) were conducted within a potential range of ±250 mV at a scanning rate of 5 $mV \cdot s^{-1}$.

2.5. Atomic force microscope analysis (AFM)

The AFM technique was used to study the morphological properties of AISI 1020 steel surface with and without poly(3-sulfolene-co-*cis*-2-butene-1,4-dilinoleate). AFM analysis was carried out using NaioAFM 2022, NanoSurf AG (Switzerland).

2.6. Theoretical evaluation

All calculations of structural parameters in this section were executed using Gaussian09 software [19]. The B3LYP 6-311 + G(d, p) method was utilized to perform comprehensive quantum chemical calculations and optimize geometric configurations. According to Koopman's theory [20], the E_{HOMO} and E_{LUMO} values are denoted by ionization potential (I) and electron affinity (A), which has reversed sign respectively.

$$I = -E_{HOMO} \tag{1}$$

$$A = -E_{LUMO} \tag{2}$$

Some chemical parameters, including electronegativity (χ), hardness (η), softness (S) and chemical potential (μ), were calculated based on density functional theory. To calculate χ, η and S, relations (3–5) were used:

$$\chi = -\mu \frac{(I + A)}{2} \tag{3}$$

$$\eta = \frac{(I + A)}{2} \tag{4}$$

$$S = \frac{1}{2\eta} \tag{5}$$

3. Results and Discussion

3.1. Characterization of the copolymer obtained

The FTIR spectrum of PSCOCBDL is illustrated in Figure 1. The peaks at 2926.81 and 2858.10 cm^{-1} correspond to aliphatic stretching vibration of C–H bonds, respectively. The peak at 1712.11 cm^{-1} corresponds to the stretching vibration of C=O in the ester group, the peak at 1120.88 cm^{-1} to the stretching vibration of C-O bonds of the ester, while the peak at 1619.17 cm^{-1} to the stretching vibration of aliphatic C=C bonds. The peaks observed at 1417.21 and 1281.02 cm^{-1} are indicative of symmetric and asymmetric stretching vibrations of S=O groups in sulfolene, respectively. The C–S bending peak corresponds to the wavenumber 648.91 cm^{-1}.

Figure 2 shows the GPC of PSCOCBDL. The molecular weights of PSCOCBDL and the polydispersity index were measured using gel permeation chromatography. The M_n (number-average molecular weight) and M_w (weight-average molecular weight) parameters of PSCOCBDL were found to be 1808 and 2219 g/mol, respectively. The peak molecular weight (M_p) of PSCOCBDL was found to be 1339 g/mol. The obtained polydispersity index (M_w/M_n) of 1.227 confirms that the polymerization is good and the number of chains is not exaggerated [21].

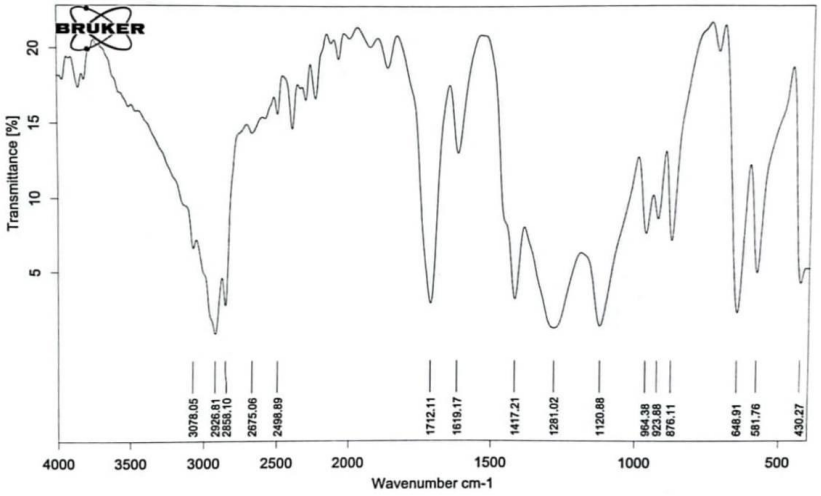

Figure 1. FTIR spectrum of PSCOCBDL copolymer.

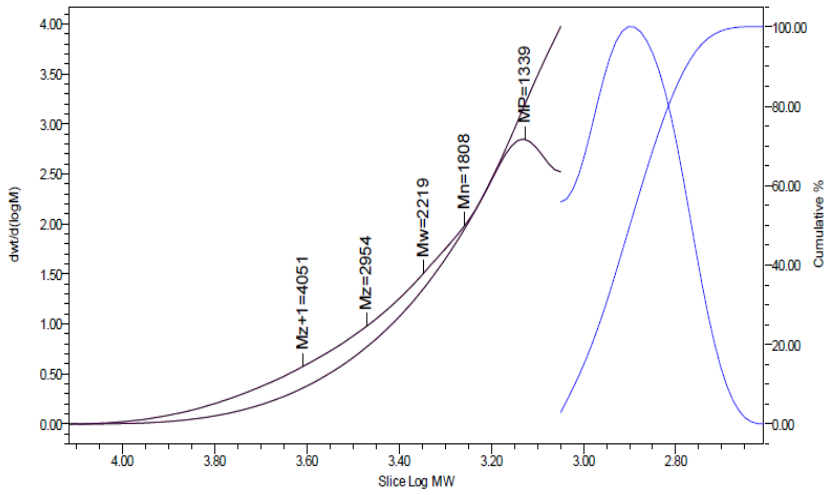

Figure 2. GPC chromatograms of PSCOCBDL copolymer.

3.2. Electrochemical measurements

3.2.1. Open circuit potential measurements (OCP)

Open circuit potential (OCP) plots were recorded for uninhibited and inhibited solutions for 30 min (until a constant potential was obtained). Figure 3 shows that the OCP of AISI 1020 steel at 298 K was attained after 30 min of exposure. It is obvious that the potential of AISI 1020 steel electrode immersed in 0.1 N HCl solution (blank curve) initially tends to more negative potentials, which represents the breakdown of the pre-immersion air-formed surface oxide film [22]. This is followed by the growth of a new oxide film in the solution, so that the potential shifts again in the noble direction until a steady state potential is established. The addition of PSCOCBDL inhibitor at a concentration of 15 ppm to the acid medium caused no difference in OCP, whereas the corrosion potential of AISI 1020 steel at concentrations of 30, 45 and 60 ppm moved in the positive direction.

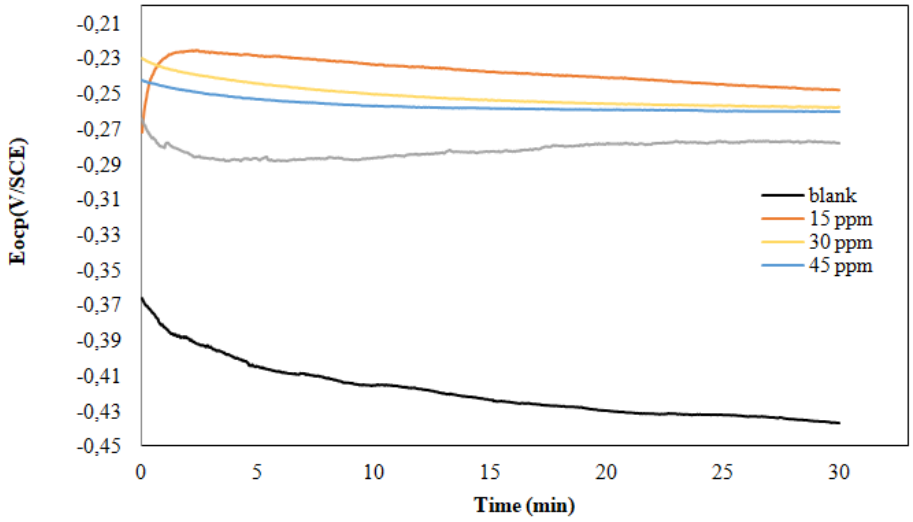

Figure 3. Open circuit potential of AISI 1020 steel in 0.1 N HCl without inhibitor and with different concentrations of PSCOCBDL.

3.2.2. Electrochemical impedance spectroscopy (EIS)

Electrochemical impedance measurements were conducted to give insights into the acid-interface kinetics of AISI 1020 steel and the manner in which the inhibitor copolymer PSCOCBDL modifies this kinetics. The Nyquist plots depicting corrosion of AISI 1020 steel in 0.1 N HCl solution at 298 K are shown in Figure 4. The plots were obtained with and without different concentrations of PSCOCBDL inhibitor. As shown by semicircles in Figure 4 of Nyquist plots, charge transfer is the primary mechanism governing the corrosion of AISI 1020 steel [23, 24]. This indicates that the protective properties of AISI 1020 steel surface are enhanced as the concentration of inhibitor copolymer causes an increase in the diameters of the semicircles. Therefore, the adsorbent layer's thickness and the dielectric properties are associated with the capacitive semicircle [25]. Figure 5 illustrates a simple equivalent circuit model that was employed to analyze derived impedance spectra. This model comprised charge transfer resistance (R_{ct}), solution resistance (R_s) and double layer capacitance (C_{dl}) given by.

$$C_{dl} = \frac{1}{2\pi f_{max} R_{ct}} \tag{6}$$

The inhibition efficiency (%*IE*) from EIS measurements was calculated from the following relation [26]:

$$\%IE = \frac{R_{ct(inh)} - R_{ct}}{R_{ct(inh)}} \cdot 100 \tag{7}$$

where R_{ct} and $R_{ct(inh)}$ are charge transfer resistance without and with inhibitor, respectively. The experimental data and results of computer fitting of the Nyquist plot using the

corresponding equivalent circuit model of 0.1 N HCl containing 45 ppm of PSCOCBDL inhibitor are demonstrated in Figure 6.

Table 1 gives the main parameters obtained from EIS such as charge transfer resistance (R_{ct}), solution resistance (R_s), double layer capacitance (C_{dl}) and inhibition efficiency (%*IE*). In the presence of various concentrations of the inhibitor copolymer PSCOCBDL, it was observed that the increase in R_{ct} and %*IE* and decrease in C_{dl} values were attributable to the formation of a protective film on the metal surface, denoting that adsorption of the inhibitor copolymer was smooth with increasing inhibitor concentration [27, 28].

Table 1. The EIS parameters for AISI 1020 steel at 0.1 N HCl without and with different concentrations of PSCOCBDL inhibitor.

Name of inhibitor	Conc. (ppm)	R_s (Ω·cm^2)	R_{ct} (Ω·cm^2)	C_{dl} (μF cm^{-2})	%*IE*
Blank	–	1.02	2.70	168.00	–
PSCOCBDL	15	0.77	39.00	32.50	93.07
	30	0.93	45.40	26.30	94.00
	45	0.95	49.00	24.50	94.48
	60	0.98	67.50	18.30	96.00

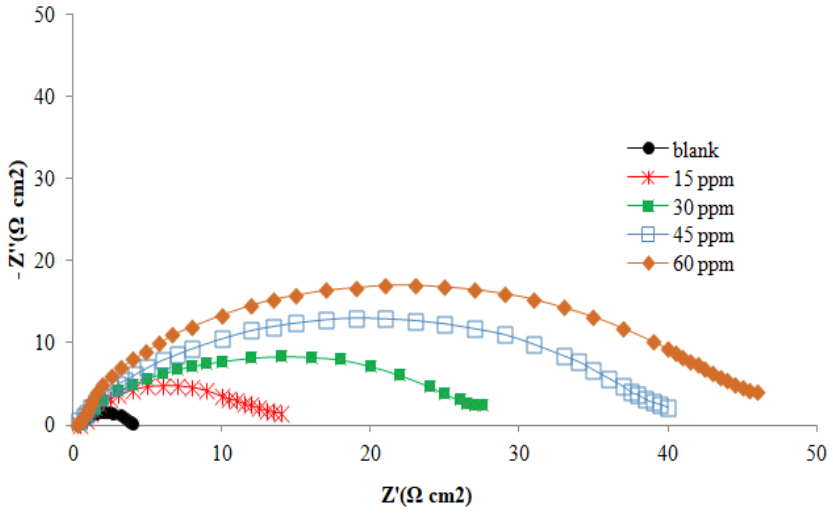

Figure 4. Nyquist plot for AISI 1020 steel in 0.1 N HCl solution without and with different concentrations of PSCOCBDL inhibitor.

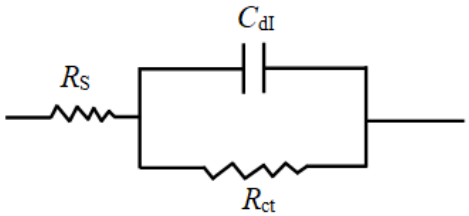

Figure 5. Equivalent circuit diagram for fitting of impedance spectra.

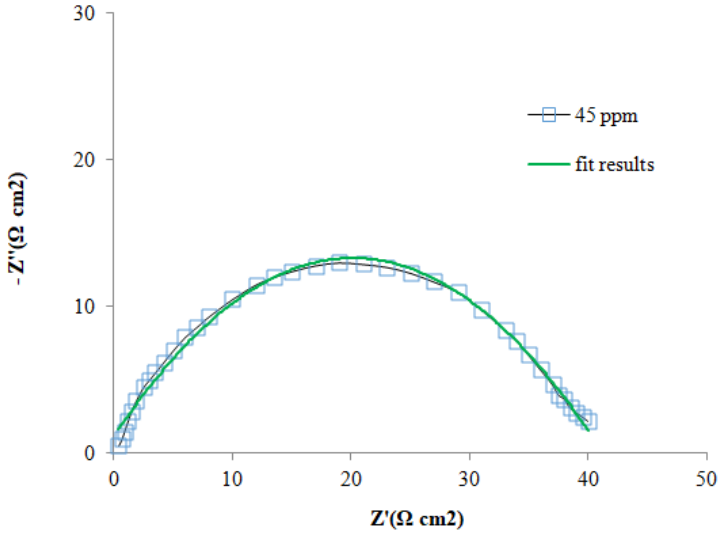

Figure 6. Experimental data and computer fitting results of Nyquist plot in 0.1 N HCl containing 45 ppm of PSCOCBDL.

3.2.3. Potentiodynamic polarization measurements

Potentiodynamic polarization (PDP) studies were performed on AISI 1020 steel samples immersed in 0.1 N HCl solutions containing different inhibitor concentrations at a temperature of 298 K. The potentiodynamic polarization curves thus obtained are presented in Figure 7. Table 2 provides a summary of electrochemical parameters acquired from polarization curves. The corrosion inhibition efficiency (%*IE*) is calculated from the corrosion rate of AISI 1020 steel according to Equation 3 [29].

$$\%IE = \frac{CR_{\text{blank}} - CR_{\text{inhib}}}{CR_{\text{blank}}} \tag{8}$$

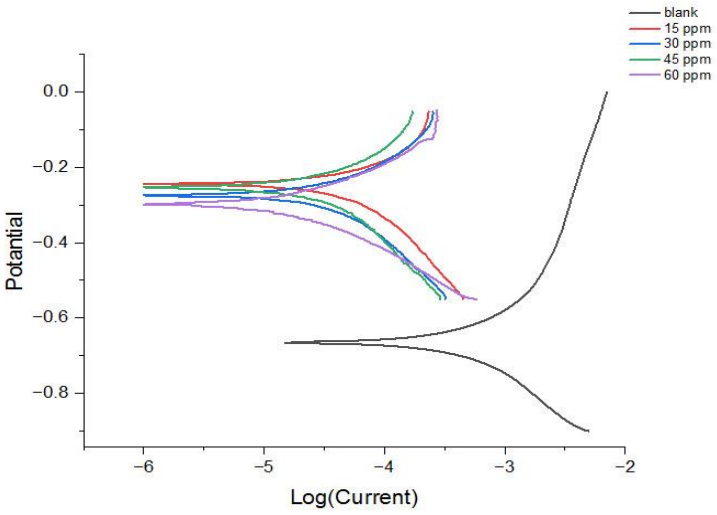

Figure 7. Potentiodynamic polarization curves measured on AISI 1020 steel in 0.1 N HCl solution with and without different concentrations of PSCOCBDL at 298 K.

Table 2. Electrochemical parameters of AISI 1020 steel in 0.1 N HCl without an inhibitor and with various concentrations of PSCOCBDL at 298 K.

Conc. (ppm)	$-E_{corr}$ (mV)	i_{corr} (mA/cm^2)	β_c (mV/dec)	β_a (mV/dec)	*CR* (mpy)	%*IE*
Blank	658.600	0.485	262	258	5.636	–
15	236.700	0.030	188	107	0.352	93.75
30	266.900	0.028	227	152	0.329	94.16
45	236.200	0.026	270	137	0.300	94.68
60	296.100	0.018	166	145	0.212	96.23

As expected, the data clearly indicate that the corrosion current density (i_{corr}) and corrosion rate (*CR*) decreased upon addition of different concentrations of PSCOCBDL inhibitor. Because of the adsorption effect of inhibitor molecules, the changes become more evident as the inhibitor concentration increases, providing the metal surface with a significant degree of protection by obstructing the active sites [30]. As seen from Table 4, the shift of the corrosion potential (E_{corr}) value after addition of PSCOCBDL inhibitor exceeds 85 mV, which may suggest cathodic or anodic type of the inhibitor [31, 32]. The E_{corr} values were found to move in the positive direction with increasing concentration of PSCOCBDL. This indicates the anodic type behavior of this prepared copolymer inhibitor at the different concentrations studied [33].

3.3. Simulation of the adsorption isotherm

Surface coverage θ was estimated from the corrosion rate of AISI 1020 steel with and without PSCOCBDL inhibitor (CR_{blank} and CR_{inhib} respectively at 25°C) according to the equation:

$$\theta = \frac{CR_{blank} - CR_{inhib}}{CR_{blank}} \tag{9}$$

In addition, several typical adsorption isotherms (Temkin, Frumkin, Flory Huggins and Langmuir isotherms) were tested. The adsorption behavior was most accurately characterized by the Langmuir isotherm as determined by the correlation coefficient values (R^2). The equation is expressed as [34]:

$$\frac{C_{inhib}}{\theta} = \frac{1}{K_{ads}} + C_{inhib} \tag{10}$$

where K_{ads} is the adsorption equilibrium constant and C_{inhib} is the concentration of the inhibitor. The Langmuir isotherm at 298 K for different concentrations of PSCOCBDL inhibitor in 0.1 N HCl is demonstrated in Figure 8. From Figure 8, the value of intercept is used to determine the K_{ads} value as in Table 3. The larger K_{ads} values indicate a strong adsorption of inhibitor molecules on the surface of AISI 1020 steel [35]. The standard free

energy of adsorption (ΔG^0_{ads}) was determined from the K_{ads} value by using the following equation [36].

$$K_{ads} = \frac{1}{55.5}\exp\left(\frac{\Delta G^0_{ads}}{RT}\right) \quad (11)$$

where 55.5 represents the concentration of water in solution in mol·L^{-1}. The adsorption model is categorized as physisorption when values of ΔG°_{ads} are around or lower than –20 kJ·mol^{-1}, whilst inhibitors work by chemisorption model when ΔG^0_{ads} is around or more negative than –40 kJ·mol^{-1} [37]. In this study, the ΔG^0_{ads} value calculated for PSCOCBDL is –34.782 kJ·mol^{-1}. This calculation demonstrates that adsorption of PSCOCBDL on AISI 1020 steel is chemisorption.

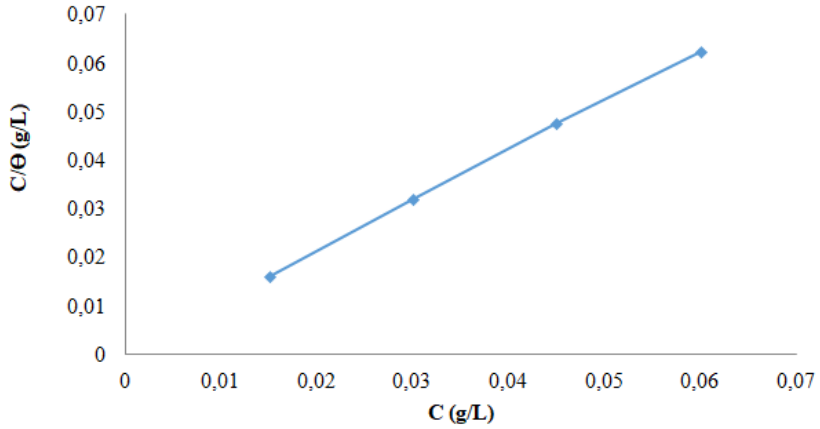

Figure 8. Langmuir adsorption for AISI 1020 steel in 0.1 N HCl solution with different concentrations of PSCOCBDL at 298 K.

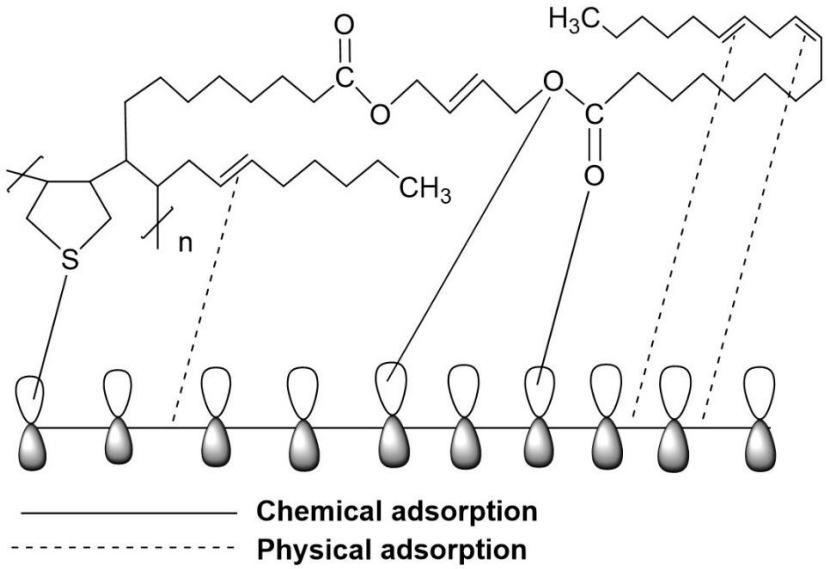

Figure 9. Suggested inhibition mechanism of PSCOCBDL of AISI 1020 steel in the acid environment.

Table 3. Adsorption equilibrium constant, correlation coefficient and standard free energy of PSCOCBDL adsorption on AISI 1020 steel in 0.1 N HCl.

Inhibitor	K_{ads} (L·g^{-1})	R^2	ΔG^0 (kJ·mol^{-1})
PSCOCBDL	1250	0.9998	–34.782

Figure 9 provides particular adsorption mechanisms that contribute to PSCOCBDL inhibitor's corrosion inhibition properties. This understanding helps to unravel the corrosion prevention function of PSCOCBDL.

3.4. Atomic force microscope analysis (AFM)

AFM is a strong technique to examine surface morphology. It has become a new option for studying the impact of an inhibitor on the generation and progression of corrosion in acid media [38]. Two dimensional (2D) and three dimensional (3D) AFM morphologies of AISI 1020 steel surface immersed in 0.1 N HCl (blank) and AISI 1020 steel surface immersed in 0.1 N HCl containing different concentrations of inhibitor copolymer PSCOCBDL are given in Figure 10(a)–(f). In AFM analysis, S_q as the root mean square, S_a as the average roughness, S_p as the maximum peak height, and S_v as the maximum pit depth are the most utilized metrics for describing the surface roughness. The results in Table 4 indicate that roughness increased in the acid medium (0.1 N HCl) because of the corrosion reaction, but in the presence of inhibitor copolymer PSCOCBDL the roughness was reduced because of adsorption of the inhibitor copolymer on AISI 1020 steel surface to form a protective layer [39]. The reduced roughness value of the PSCOCBDL copolymer at 60 ppm concentration compared to that at 45 ppm reveals that the PSCOCBDL inhibitor at 60 ppm concentration protects the AISI 1020 steel surface more efficiently than at 45 ppm concentration in 0.1 N HCl solution.

Table 4. AFM parameters of AISI 1020 steel at 0.1 N HCl with and without different concentrations of PSCOCBDL inhibitor.

Name of the inhibitor	Conc. (ppm)	S_q (nm)	S_a (nm)	S_p (nm)	S_v (nm)
blank	–	324.5	266.9	883.2	816.1
PSCOCBDL	45	266.5	207.7	786.9	787.6
	60	133.0	106.9	395.8	461.3

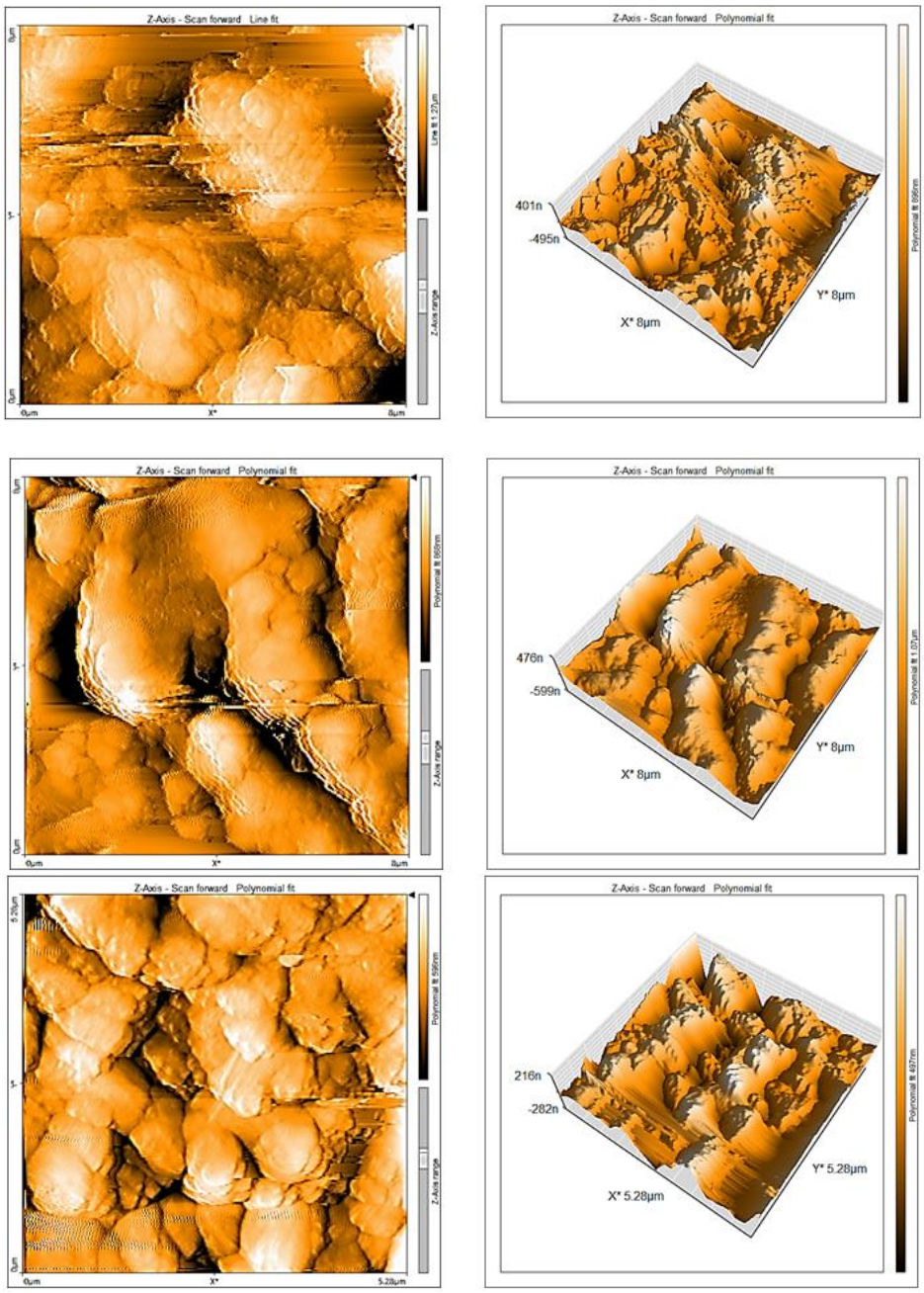

Figure 10. AFM 2D & 3D images of AISI 1020 steel in 0.1 N HCl (a) and (b) in the absence of inhibitor, (c) and (d) in the presence of 45 ppm PSCOCBDL, (e) and (f) in the presence of 60 ppm PSCOCBDL.

3.5. Theoretical results

The optimized geometry, HOMO and LUMO of the synthesized copolymer (PSCOCBDL) determined in this work are presented graphically in Figure 11. The parameters of this copolymer such as E_{HOMO}, E_{LUMO}, ΔE, E_{Total}, ionization potential (I), electron affinity (A), electronegativity (χ), hardness (η), softness (S), and chemical potential (μ) determined by quantum chemical calculations are listed in Table 5.

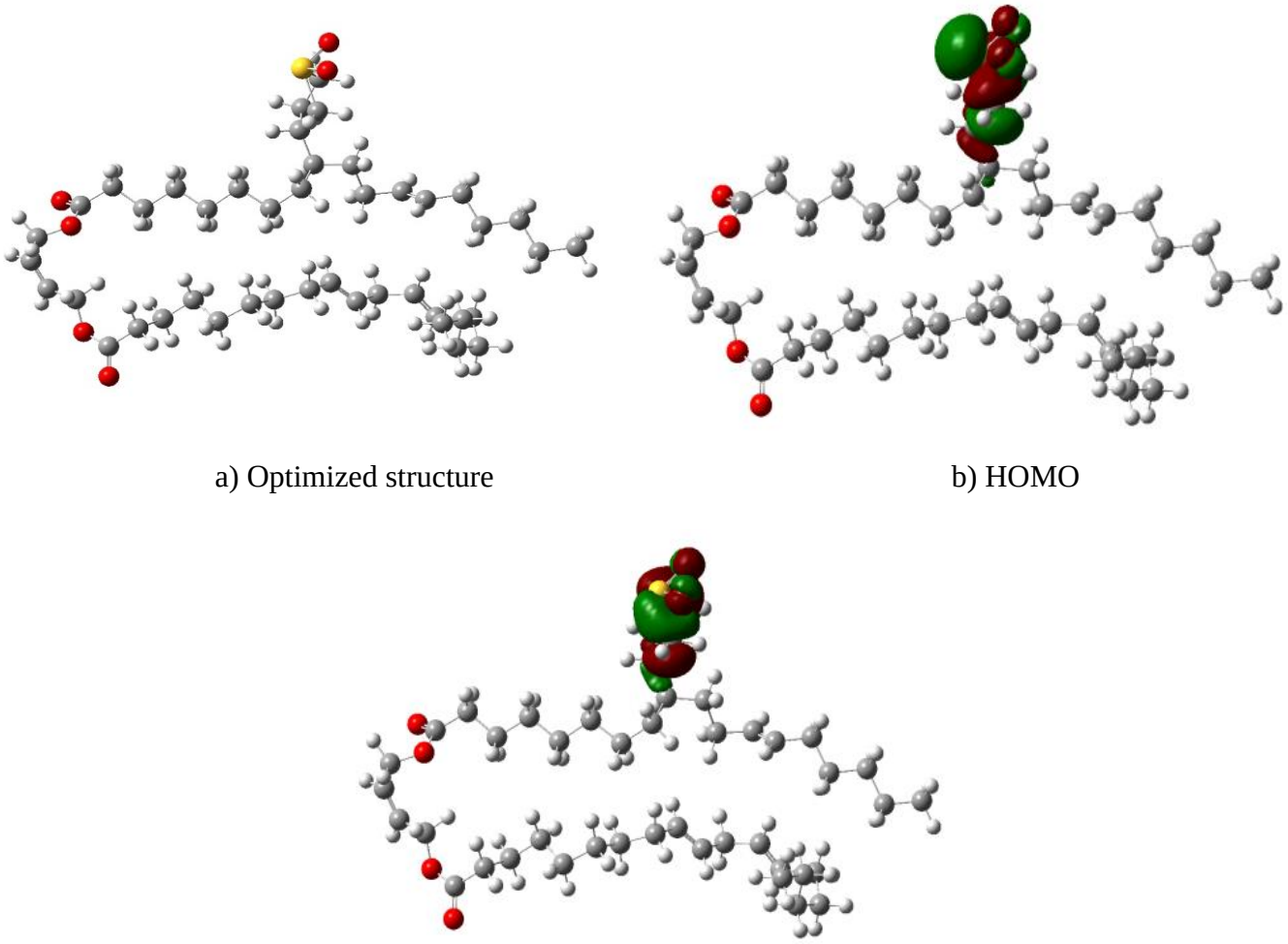

a) Optimized structure b) HOMO

c) LUMO

Figure 11. Optimized structure (a), HOMO (b) and LUMO (c) of PSCOCBDL copolymer**.**

Table 5. Quantum chemical characteristics of PSCOCBDL inhibitor molecule.

E_{HOMO} (eV)	E_{LUMO} (eV)	ΔE_{gap} (eV)	E_{Total} (eV)	I (eV)	A (eV)	χ (eV)	η (eV)	S (eV)	M (eV)
–8.568	–2.503	6.065	–5.562	8.568	2.503	5.535	3.032	0.165	–5.535

According to Koopman's theorem, the ability of molecules to donate electrons can be reliably predicted using these energies. Literature study indicates that adsorption of inhibitor on the metal surface can occur due to donor–acceptor interactions between lone pairs and/or π electrons of the inhibitor molecules with the d-orbitals of metal surface atoms, leading to stronger adsorption of inhibitor molecules on the surface, thus the protective layer is formed [40, 41]. A molecule with a higher E_{HOMO} can speedily take electrons from a suitable acceptor molecule with a lower-energy vacuous molecular orbital [42], while the E_{LUMO} value indicates how well the molecule can donate electrons. Hardness (η) is defined as a

measure of variation in chemical potential over the overall number of atoms, one of key specifics in corrosion investigations [43]. As hardness (η) increases, the molecule becomes more stable, while softness (*S*) is the opposite of hardness. These results are in good agreement with experimental ones.

Conclusions

In this investigation, poly(3-sulfolene-co-*cis*-2-butene-1,4-dilinoleate) (PSCOCBDL) inhibitor prepared was sturdy in inhibiting corrosion of AISI 1020 steel. The electrochemical techniques demonstrate that the inhibition efficiency amounts to 96% at 298 K in the presence of PSCOCBDL inhibitor at a concentration of 60 ppm. The corrosion inhibition efficiency was shown to increase with the concentration of the copolymer inhibitor. Potentiodynamic polarization measurements detected that PSCOCBDL was an anodic type corrosion inhibitor. The PSCOCBDL copolymer adsorption on the metal was shown to occur as chemisorption and fit the Langmuir adsorption isotherm. The AFM investigation denoted that PSCOCBDL inhibitor molecules are adsorbed on AISI 1020 steel surface and protect AISI 1020 steel against corrosion. The results acquired from the experiments agree with those of the theoretical study.

References

1. L.D. Sarno, A. Majidian and G. Karagiannakis, The Effect of Atmospheric Corrosion on Steel Structures: A State-of-the-Art and Case-Study, *Buildings*, 2021, **11**, 571. doi: 10.3390/buildings11120571
2. A.H. Al-Moubaraki and I.B. Obot, Corrosion challenges in petroleum refinery operations: Sources, mechanisms, mitigation, and future outlook, *J. Saudi Chem. Soc*., 2021, **25**, 101370. doi: 10.1016/j.jscs.2021.101370
3. Y.M. Abdulsahib, A.J.M. Eltmimi, S.A. Alhabeeb, M.M. Hanoon, A.A. Al-Amiery, T. Allami and A.A.H. Kadhum, Experimental and theoretical investigations on the inhibition efficiency of N-(2,4-dihydroxytolueneylidene)-4-methylpyridin-2-amine for the corrosion of mild steel in hydrochloric acid, *Int. J. Corros. Scale Inhib*., 2021, **10**, no. 3, 885–899. doi: 10.17675/2305-6894-2021-10-3-3
4. C. Mahmou, E.M. Bouissoui, F. Bouhlal, N. Labjar, I. Merimi, S. Kaya, B. El Ibrahimi, M. Chellouli, A. Dahrouch and S. El Hajjaji, Synergistic effects of aminotris (methylene phosphonic acid) and Zn^{2+} on the carbon steel corrosion in acid media: An experimental and theoretical approach, *Int. J. Corros. Scale Inhib*., 2021, **10**, no. 3, 1245–1281. doi: 10.17675/2305-6894-2021-10-3-24
5. O.S.I. Fayomi, A.E. Olawuni and I.G. Akande, Studies on Phosphorus-Alumunum Oxide coating effects on mild steel microstructure, corrosion and mechanical behavior, *Port. Electrochim. Acta*, 2023, **41**, 315–326. doi: 10.4152/pea.2023410405

6. A.A. Naser, A.S. Al-Mubarak and H.Z. Al-Sawaad, Synthesis, characterization and evaluation of some graphene oxide derivatives and their application as corrosion inhibitors for carbon steel alloy type C1025 in hydrochloric acid, *Int. J. Corros. Scale Inhib*., 2019, **8**, no. 4, 974–997. doi: 10.17675/2305-6894-2019-8-4-11
7. C. Verma, E.E. Ebenso, M.A. Quraishi and C.M. Hussain, Recent developments in sustainable corrosion inhibitors: design, performance and industrial scale applications, *Mater. Adv*., 2021, **2**, 3806–3850. doi: 10.1039/D0MA00681E
8. L. Chen, D. Lu and Y. Zhang, Organic Compounds as Corrosion Inhibitors for Carbon Steel in HCl Solution: A Comprehensive Review, *Materials*, 2022, **15**, 2023. doi: 10.3390/ma15062023
9. M.D. Plotnikova, A.B. Shein, M.G. Shcherban and A.D. Solovyev, The study of thiadiazole derivatives as potential corrosion inhibitors of low-carbon steel in hydrochloric acid, *Bulletin of the University of Karaganda - Chemistry*, 2021, **103**, 93–102. doi: 10.31489/2021Ch3/93-102
10. H.M. Abd El-Lateef and M.A.A. Ali, Divinyl sulfone cross-linked β-cyclodextrin polymer as new and effective corrosion inhibitor for Zn anode in 3.5 M KOH, *Trans. Indian Inst. Met*., 2016, **69**, 1783–1792. doi: 10.1007/s12666-016-0838-3
11. A.A. Al-Amiery, W.N.R.W. Isahak and W.K. Al-Azzawi. Corrosion Inhibitors: Natural and Synthetic Organic Inhibitors, *Lubricants*, 2023, **11**, 174. doi: 10.3390/lubricants11040174
12. X. Ma, X. Sun, M. Chang, Q. Liu, X. Dong, Y. Fan and R. Chen, Adsorption of Different Ionic Types of Polyacrylamide on Montmorillonite Surface: Insight from QCM-D and Molecular Dynamic Simulation, *Molecules*, 2023, **28**, 4417. doi: 10.3390/molecules28114417
13. A.A. Aly, A.A. Khalil, M.N. Ismail, S.A. Abd El-Kader and M.M. Eldesouky, Synthesis of some polymers containing heterocyclic rings corrosion inhibitors of mild steel, *Egypt. J. Chem*., 2016, **59**, 745–757.
14. D.Q. Huong, T. Duong and P.C. Nam, Effect of the Structure and Temperature on Corrosion Inhibition of Thiourea Derivatives in 1.0 M HCl Solution, *ACS Omega*, 2019, **4**, 14478–14489. doi: 10.1021/acsomega.9b01599
15. H.T. Rahal, A.M. Abdel-Gaber and G.O. Younes, Inhibition of steel corrosion in nitric acid by sulfur containing compounds, *Chem. Eng. Commun*., 2016, **203**, 435–445. doi: 10.1080/00986445.2015.1017636
16. A.C.D. Pfluck, D.P.C. de Barros and L.P. Fonseca, Biodegradable Polyester Synthesis in Renewed Aqueous Polycondensation Media: The Core of the New Greener Polymer-5B Technology, *Processes*, 2021, **9**, 365. doi: 10.3390/pr9020365
17. M.R. Elkatory, M.A. Hassaan, E.A. Soliman, V.C. Niculescu, M.S. Raboaca and A. El Nemr, Influence of Poly (benzyl oleate-co-maleic anhydride) Pour Point Depressant with Di-Stearyl Amine on Waxy Crude Oil, *Polymers*, 2023, **15**, 306. doi: 10.3390/polym15020306

18. Z. Wang, Y. Zhao and Y. Wei, Syntheses and properties of tri-andmulti-block copolymers consisting of polybutadiene and polylactide segments, *RSC Adv*., 2022, **12**, 29777–29784. doi: 10.1039/D2RA05051J
19. F. Tezcan, G. Yerlikaya, A. Mahmood and G. Karda, A novel thiophene Schiff base as an efficient corrosion inhibitor for mild steel in 1.0 M HCl: Electrochemical and quantum chemical studies, *J. Mol. Liq*, 2018, **269**, 398–406. doi: 10.1016/j.molliq.2018.08.025
20. J. Luo, Z.Q. Xue, W.M. Liu, J.L. Wu and Z.Q. Yang, Koopmans' Theorem for Large Molecular Systems within Density Functional Theory, *J. Phys. Chem. A*., 2006, **110**, 12005–12009. doi: 10.1021/jp063669m
21. B. Al-Mayyahi, H. Al-Lami and A. Haddad, Synthesis of some Nano Multi Arms Polylactide-Dipentaerythritol Organic Polymers, *J. Mex. Chem. Soc*., 2020, **64**, 253–263. doi: 10.29356/jmcs.v64i4.1182.
22. L.W. El Khatib, H.T. Rahal and A.M. Abdel-Gaber, Synergistic Effect between Fragaria ananassa and Cucurbita pepo L Leaf Extracts on Mild Steel Corrosion in Hydrochloric Acid Solutions, *Prot. Met. Phys. Chem. Surf*., 2020, **56**, 1096–1106. doi 10.1134/S2070205120050111
23. M.D. Plotnikova, A.D. Shitoeva, A.D. Solovyev, A.N. Bakiev and A.B. Shein, Some aspects of the of the mechanism of C1018 steel protection in hydrochloric acid solutions by triazole derivatives, *Int. J. Corros. Scale Inhib*., 2023, **12**, no. 2, 511–530. doi: 10.17675/2305-6894-2023-12-2-8
24. S. Bashir, V. Sharma, P. Dhaundiyal, N. Shafi and A. Kumar, Gymneme Sylvestre as a Green Corrosion Inhibitor for Aluminum in an Acidic Medium, *Port. Electrochim. Acta*, 2021, **39**, 199–212. doi: 10.4152/pea.2021390304
25. M. Abdallah, A. Fawzy and M. Alfakeer, Inhibition Potentials and Adsorption Performance of Two Sulfonylurea Antibiotic Expired Drugs on the Corrosion of Mild Steel in 0.5 M H_2SO_4, *Int. J. Electrochem. Sci*., 2020, **15**, 10289–10303. doi: 10.20964/2020.10.37
26. R.S. Abdel Hameed, A.H. Al-Bagawi, H.A. Shehata, A.H. Shamroukh and M. Abdallah, Corrosion Inhibition and Adsorption Properties of Some Heterocyclic Derivatives on C- Steel Surface in HCl, *J. Bio Tribo Corros*., 2020, **6**, 51. doi: 10.1007/s40735-020-00345-y
27. M.A. Quraishi, S.Ch. Dheeraj and S.S. Viswanathan, *Heterocyclic Organic Corrosion Inhibitors: Principles and Applications*, Elsevier, 2020, 284.
28. A. Khadraoui, A. Khelifa, M. Hadjmeliani, R. Mehdaoui, K. Hachama, A. Tidu, Z. Azari, I.B. Obot and A. Zarrouk, Extraction, characterization and anti-corrosion activity of Mentha pulegium oil: Weight loss, electrochemical, thermodynamic and surface studies, *J. Mol. Liq*., 2016, **216**, 724–731. doi: 10.1016/j.molliq.2016.02.005
29. T.A.S. Guimarães, J.N. da Cunha, G.A. de Oliveira, T.U. da Silva, S,M. de Oliveira, J.R. de Araújob, S.P. Machadoa, E. D'Elia and M.J.C. Rezende, Nitrogenated derivatives of furfural as green corrosion inhibitors for mild steel in HCl solution, *J. Mater. Res. Technol*., 2020, **9**, 7104–7122. doi: 10.1016/j.jmrt.2020.05.019

30. S.A.X. Stango and U. Vijayalakshmi, Studies on corrosion inhibitory effect and adsorption behavior of waste materials on mild steel in acidic medium, *J. Asian Ceram. Soc*., 2018, **6**, 20–29. doi: 10.1080/21870764.2018.1439608
31. A. Fiala, W. Boukhedena, S.E. Lemallem, H.B. Ladouani and H. Allal, Inhibition of Carbon Steel Corrosion in HCl and H_2SO_4 Solutions by Ethyl 2-Cyano-2-(1,3-dithian-2-ylidene) Acetate, *J. Bio Tribo Corros*., 2019, **5**, 42. doi: 10.1007/s40735-019-0237-5
32. A. Visa, N. Plesu, B. Maranescu, G. Ilia, A. Borota and L. Crisan, Combined Experimental and Theoretical Insights into the Corrosion Inhibition Activity on Carbon Steel Iron of Phosphonic Acids, *Molecules*, 2021, **26**, 19. doi: 10.3390/molecules26010135
33. H.J. Habeeb, H.M. Luaibi, R.M. Dakhil, A.A.H. Kadhum, A.A. Al-Amiery and T.S. Gaaz, Development of new corrosion inhibitor tested on mild steel supported by electrochemical study, *Results Phys*., 2018, **8**, 1260–1267. doi: 10.1016/j.rinp.2018.02.015
34. A.E. Vazquez, L.A.L. Reséndiz, I.A. Figueroa, F.J.R. Gómez, M. Figueroa, D.Á. Beltrán, M. Castro and A. Miralrio, Corrosion inhibition assessment on API 5L X70 steel by preussomerin G immersed in saline and saline acetic, *J. Adhes. Sci. Technol*., 2021, **35**, 873–899. doi: 10.1080/01694243.2020.1826828
35. A.A. Alamiery, W.N.R.W. Isahak, H.S.S. Aljibori, H.A. Al-Asadi and A.A.H. Kadhum, Effect of the structure, immersion time and temperature on the corrosion inhibition of 4-pyrrol-1-yl-N-(2,5-dimethyl-pyrrol-1-yl)benzoylamine in 1.0 M HCL solution, *Int. J. Corros. Scale Inhib*., 2021, **10**, no. 2, 700–713. doi: 10.17675/2305-6894-2021-10-2-14
36. A. Batah, A. Anejjar, L. Bammou, M. Belkhaouda and R. Salghi, Effect of Apricot Almond Oil as Green Inhibitor for Steel Corrosion in Hydrochloric Media, *Por Electrochim. Acta*, 2020, **38**, 201–214. doi: 10.4152/pea.202004201
37. Y. Xu, S. Zhang, W. Li, L. Guo, S. Xu, L. Feng and L.H. Madkour, Experimental and theoretical investigations of some pyrazolo-pyrimidine derivatives as corrosion inhibitors on copper in sulfuric acid solution, *Appl. Surf. Sci*., 2018, **459**, 612–620. doi: 10.1016/j.apsusc.2018.08.037
38. M.M. Motawea, Corrosion Inhibition Effect of Expired Levothyroxine Drug on Stainless Steel 304L in 0.5 M H_2SO_4 Solution, *Int. J. Electrochem. Sci*., 2021, **16**, 21021. doi: 10.20964/2021.02.17
39. N. Anitha, A.U. Maheswari, L. Ilakiya, J.A. Joency, K. Bhuvaneswari, G. Gomathi, M. Lavanya, S. Susithra, X. Susmitha, S. Rajendran, V. Velkannan, G. Singh and C. Lacnjevac, Corrosion resistance of orthodontic wire made of Gold 18K alloy in artificial saliva in the presence of Éclairs milky candy, *Int. J. Corros. Scale Inhib*., 2023, **12**, no. 2, 664–678. doi: 10.17675/2305-6894-2023-12-2-15
40. O. Olivares, N.V. Likhanova, B. Gomez, J. Navarrete, M.E. Llanos-Serrano, E. Arce and J.M. Hallen, Electrochemical and XPS studies of decylamides of α-amino acids adsorption on carbon steel in acidic environment, *Appl. Surf. Sci*., 2006, **252**, 2894–2909. doi: 10.1016/j.apsusc.2005.04.040

41. A. Popova, E. Sokolova, S. Raicheva and M. Christov, AC and DC study of the temperature effect on mild steel corrosion in acid media in the presence of benzimidazole derivatives, *Corros. Sci*., 2003, **45**, 33–58. doi: 10.1016/S0010-938X(02)00072-0
42. G. Karthik, M. Sundaravadivelu and P. Rajkumar, Corrosion inhibition and adsorption properties of pharmaceutically active compound esomeprazole on mild steel in hydrochloric acid solution, *Res. Chem. Intermed*., 2015, **41**, 1543–1558. doi: 10.1007/s11164-013-1291-0
43. S.A. Umoren, M.M. Solomon, S.A. Ali and H.D.M. Dafalla, Synthesis, Characterization, and Utilization of a Diallylmethylamine-Based Cyclopolymer for Corrosion Mitigation in Simulated Acidizing Environment, *Mater. Sci. Eng. C*, 2019, **100**, 897–914. doi: 10.1016/j.msec.2019.03.057

♦ ♦ ♦